Sustainable Food Technology

ROYAL SOCIETY OF CHEMISTRY

PAPER

View Article Online
View Journal

Cite this: DOI: 10.1039/d5fb00392j

Formation and characteristics of large yellow croaker (*Pseudosciaena crocea*) roe protein isolates/gellan gum composite gels: effects of pH and mass ratio

Yi-Nan Du, Jiao Jia, Zhi-Wen Lin, Shu-Xun Yang, Jia-Nan Yan and Hai-Tao Wu *

Large yellow croaker (*Pseudosciaena crocea*) roe protein isolates are excellent marine-derived functional proteins. To expand the application of pcRPI in the food industry, the effects of pH and mass ratio on the complex coacervation of pcRPI with gellan gum (Gg) was discussed. According to the turbidity titration results, the pH values for the formation of soluble complexes and complex coacervates increased and then tended to plateau with an increase in the pcRPI/Gg mass ratio. Moreover, the pcRPI/Gg gels were prepared at a pcRPI : Gg mass ratio of 10 : 1 at different pH values chosen from different phases (6, 8 and 10). The pcRPI/Gg formed a gel at pH 6, showing the highest storage modulus (G') value, which was 2.5-fold and 12.1-fold higher than those at pH 8 and pH 10, respectively. The addition of Gg significantly improved the gelation behavior of pcRPI, enabling stable gel formation at pH 6, a condition under which the protein alone could not form a gel. The molecular simulation results revealed the binding patterns between pcRPI and Gg under different pH conditions, highlighting the critical role of hydrogen bonding in stabilizing the complexes. This study offers theoretical guidance for the application of pcRPI and Gg based coacervation in the field of food gels.

Received 17th July 2025
Accepted 15th January 2026

DOI: 10.1039/d5fb00392j

rsc.li/susfoodtech

Sustainability spotlight

As we know, the aquaculture of the large yellow croaker has rapidly expanded in many countries in recent decades. In 2024, the production of large yellow croaker (*Pseudosciaena crocea*) has exceeded 292 thousand tons in China. However, a mass of roe, accounting for about 20% of the fish weight, is produced as the low-value by-product, which is usually used as animal feed. In our previous studies, we demonstrated that pcRPI is mainly composed of vitellogenin, having great functional capacities. The development of methods to convert edible large yellow croaker waste into functional ingredients will not only reduce environmental contamination but also generate significant profits for the large yellow croaker industry. This study may provide more information and guidance for the sustainable utilization of large yellow croaker resources and provide new ideas for the development of food gels.

1 Introduction

Proteins and polysaccharides are the main biopolymer macromolecules in food systems, and their interactions play a crucial role in determining food texture, stability and processing performance. Complex coacervates formed by protein–polysaccharide interactions generally exhibit improved functional properties compared with individual components.[1] Recently, many studies have focused on common proteins, such as whey protein[2] and soy protein,[3] along with various polysaccharides. In aquatic protein systems, previous studies have found that the formation of composite gels from fish proteins and polysaccharides typically requires a certain concentration or the presence of salt ions, such as Spanish mackerel myosin/yeast β-glucan[4] and grass carp myofibrillar protein/starch.[5] Therefore, it is necessary to develop a fish protein–polysaccharide composite system that can form gels at a lower concentration without the need for a salt.

Generally, when proteins and polysaccharides are physically mixed, their interactions can either be attractive or repulsive, resulting in the formation of two phases: thermodynamically incompatible and thermodynamically compatible, depending on factors such as ionic strength, pH, biopolymer type, concentration, mass ratio, and temperature.[6,7] Among these, pH and mass ratio are especially critical, as they regulate the ionization state of biopolymers and the availability of interaction sites, thereby controlling the formation of soluble complexes or phase-separated coacervates.[8,9] Igartúa *et al.*[10] investigated the phase behavior of pea protein isolate and soluble soybean polysaccharide mixtures in response to changes in the pH and

SKL of Marine Food Processing & Safety Control, National Engineering Research Center of Seafood, Collaborative Innovation Center of Seafood Deep Processing, Key Laboratory of Aquatic Product Processing and Quality Control, School of Food Science and Technology, Dalian Polytechnic University, Dalian, China. E-mail: wht205@163.com; Fax: +86-411-86318655; Tel: +86-411-86318731

mass ratio, and they found that the addition of soluble soybean polysaccharide enhanced the protein solubility and stabilized the colloidal system. Although experimental techniques such as spectroscopy and calorimetry have been widely used to investigate these interactions, they provide limited insight into molecular-scale interaction mechanisms. Molecular simulation offers a complementary approach by enabling direct visualization of binding patterns and interaction forces. Zhang *et al.*[11] comprehensively analyzed the interaction mechanisms between chickpea protein isolate and dextran by multispectral analysis and molecular docking. However, studies on the interaction between aquatic proteins and polysaccharides using a combination of experimental and computational methods from multiple perspectives are limited.

The large yellow croaker (*Pseudosciaena crocea*) is a significant species in aquaculture, owing to its great economic value and nutritional benefits. Roe is a by-product of *P. crocea* processing and is rich in protein. The protein isolates from *P. crocea* roes (pcRPI) are mainly composed of vitellogenin, and they show excellent functional properties, including strong gel-forming ability, high emulsifying capacity and oil-holding capacity, compared with soy protein isolates.[12,13] Several studies have also indicated that coacervates formed between protein and polysaccharides exhibit desirable textural and structural properties, which also enhance the gel properties of proteins.[14] Gellan gum (Gg) is an anionic polysaccharide produced by the bacterium *Sphingomonas elodea*,[15] having a low gelling concentration and a wide range of applications.[16] Gg also exhibits a good effect in improving the characteristics of protein gels, including potato protein,[17] whey protein isolate,[18] pea protein,[19] fish gelatin[20] and tilapia proteins.[21] Our previous study demonstrated that compared to cold-set whey protein/chitosan hydrogels[22] and egg white protein/dextran sulfate hydrogels,[23] the cold-set pcRPI/Gg hydrogels at lower concentration showed great gel properties.[24] However, the link between phase separation, molecular interactions and gel properties in pcRPI/Gg systems remains unclear. It is hypothesized that the phase-separation behavior of the pcRPI/Gg system governs the intermolecular interactions and network formation and that complex coacervation under appropriate pH enhances gel stability and strength.

This study intends to develop a novel gel system based on pcRPI and Gg. First, the phase-separation behavior of pcRPI and Gg was systematically modulated by adjusting the mass ratio and pH, and the gel properties of the pcRPI/Gg gels were also investigated. The rheological properties, water migration and microstructure of the pcRPI/Gg gels formed at different phases were determined using a rheometer, low field-nuclear magnetic resonance (LF-NMR) relaxometry and cryo-scanning electron microscopy (cryo-SEM). Molecular dynamics simulations were further used to analyze the interaction mechanisms between pcRPI and Gg under different pH conditions.

2 Materials and methods

2.1 Materials and chemicals

Large yellow croaker roes (pcRs) were provided by Qingdao Yujie Group Co., Ltd (Qingdao, China). The Gg was purchased from Macklin Biochemical Co., Ltd (Shanghai, China). All other chemicals used in this research were of analytical grade.

2.2 Preparation of pcRPI

The pcR powder (10%, w/v) was dispersed in a NaCl solution (0.6 M), stirred at 400 rpm for 2 h, and then centrifuged at 8000 rpm for 15 min. The supernatant was collected, the lipid from the top layer was skimmed off, and the solid residue was extracted again using the same method. The supernatant was mixed, dialyzed and lyophilized to obtain pcRPI. The purity of the pcRPI was 80.5%, and the isoelectric point of pcRPI was around pH 5.6.[12]

2.3 Preparation of pcRPI/Gg mixture solutions and heat-induced pcRPI/Gg gels

Stock Gg and pcRPI solutions at a concentration of 1.5 mg mL^{-1} were prepared by mixing Gg and pcRPI powder in deionized water. Binary dispersions were assembled by adding appropriate Gg solutions into the pcRPI solutions with pcRPI/Gg mass ratios of 30 : 1, 20 : 1, 15 : 1, 10 : 1, 5 : 1, 2 : 1, 1 : 1, 1 : 2, and 1 : 5 (w/w) to achieve a total biopolymer concentration of 1.5 mg mL^{-1}.

For the samples to be used for rheology, LF-NMR relaxometry and cryo-SEM measurements, the total biopolymer concentration was maintained at 55 mg mL^{-1} with a pcRPI/Gg mass ratio of 10 : 1. The pH values of the mixture solutions were adjusted to 10.0, 8.0 and 6.0 with NaOH or HCl solutions. Finally, gelation was induced by heating at 85 °C for 20 min. The resulting gels were then stored at −4 °C until further analysis.

2.4 Turbidity measurement

Following the procedure reported by Yan *et al.*,[25] the turbidity changes of different mixture solutions were determined. Briefly, the pH values of the pcRPI, Gg and pcRPI/Gg solutions were adjusted to pH 10 using NaOH solutions, and different concentrations of HCl solution were used to change the pH of the mixed solution. Turbidity during acidification from pH 10 to pH 1 was measured at 500 nm using a microplate reader (Infinite 200 NANO, Tecan, Switzerland), and turbidimetric titration was performed by gradually adding HCl during acidification.

2.5 Rheological properties

Frequency sweep tests were conducted over the frequency range of 0.1 to 10 Hz, with a gap of 1 mm in the rheometer (Discovery HR-1, TA Instruments Menu Co., Ltd, USA) according to Du *et al.*[26] A strain of 0.3%, chosen from the linear viscoelastic region, was applied, and the storage modulus (G') and loss modulus (G'') were recorded. The fluctuation of G'/G'' as a function of angular frequency was noted, and it aligned with a power-law equation.

$$G' = k'\omega^{n'}$$

$$G'' = k''\omega^{n''}$$

where k' and k'' are the constants associated with the power law, ω is the angular frequency (rad s^{-1}) and n' and n'' represent the frequency exponents.

2.6 Texture profile analysis

Different gels were sliced into cylinders. Texture analysis was conducted using a TA-XT Plus texture analyzer (Stable Micro Systems, Godalming, UK). The P/50 probe was used for texture profile analysis (TPA). The test parameters were as follows: pre-test speed of 1.5 mm s^{-1}, test speed of 1 mm s^{-1}, post-test speed of 1 mm s^{-1}, compression percentage of 40%, and trigger force of 5 g. The experiment was conducted at room temperature.

2.7 LF-NMR relaxometry

The water distribution of various gels was assessed using an LF-NMR analyzer (MesoMR23-060V-1, Niumag Co., Ltd, Shanghai, China) equipped with a 0.5 T permanent magnet, in accordance with our previous research.[26] The test parameters were configured as follows: τ-value = 100, the number of echoes NECH = 5000, and TW = 3000 ms. The transverse relaxation time (T_2) was also collected. Each sample was measured at least three times.

2.8 Cryo-SEM

The microstructure of various gels was examined using cryo-scanning electron microscopy (Hitachi Co., Ltd, Tokyo, Japan), following the methodology described by Yan *et al.*[27] Briefly, the samples were plunge-frozen, freeze-fractured, sublimated, and then sputter-coated with Pt in the cryo-preparation chamber (PP3010T cryo-SEM preparation system, Quorum Technologies, UK). A SU8010 SEM system (Hitachi Co., Ltd, Tokyo, Japan) was employed to observe different gels at an accelerating voltage of 10.0 kV, and micrographs were captured at 2000× magnification. The vessel percentage area (VPA), total number of junctions (TNJ) and lacunarity of cryo-SEM images were also analyzed by the AngioTool64 software.

2.9 Molecular docking

Molecular docking analysis was conducted with modifications based on previous reports.[28,29] Vitellogenin protein structures were generated *via* homology modeling using the Swiss-Model server (https://swissmodel.expasy.org/), while the Gg structure was retrieved from the PubChem database. To prepare for docking, water molecules were eliminated from the crystal structures of vitellogenin, followed by the addition of hydrogen atoms. Molecular docking was executed using the Glide module in the Schrödinger Maestro software, and the docking scores were calculated.

A comprehensive analysis of the electrostatic potential of vitellogenin at pH 6, 8, and 10 was also conducted. Specifically, the protonation states of all ionizable residues of vitellogenin at pH 6, 8, and 10 were first determined using the H++ web server. The resulting pH-specific structures were then used to calculate the electrostatic surface potential *via* the Adaptive Poisson–Boltzmann Solver (APBS) tool and were visualized in PyMOL.

2.10 Molecular dynamics simulation

Molecular dynamics (MD) simulations were executed using Desmond version 2020, following the method of Umashankar *et al.*[30] The OPLS3e force field was employed for the MD simulations, and the system was solvated with the TIP3P water model. Ions were added to neutralize the system. The energy minimization of the entire system was performed using the OPLS3e force field (an all-atom force field). The SHAKE algorithm was used to constrain the geometry of water molecules, as well as the bond lengths and angles of heavy atoms. Periodic boundary conditions were implemented to simulate a continuous system, and long-range electrostatics were handled using the Particle Mesh Ewald (PME) method. The system was equilibrated in an *NPT* ensemble at 300 K and 1.0 bar, with temperature and pressure regulated employing the Berendsen coupling algorithm. During the final preparation, the simulation was run for 100 ns with a 1.2 fs timestep, and trajectory snapshots were recorded every 100 ps, generating 10 000 frames in total. Root mean square deviation (RMSD), root mean square fluctuation (RMSF), and the number of hydrogen bonds were analyzed.

2.11 Statistical analysis

All the data are expressed as the mean ± standard deviation (n = 3). The level of significance ($p < 0.05$) was determined by the SPSS 11.5 software.

3 Results and discussion

3.1 Phase-separation behavior of pcRPI/Gg complex coacervation

Generally, the formation of complex coacervates involving proteins and polysaccharides is governed by intermolecular interactions and is influenced by pH and the mass ratio.[31] The turbidity of pcRPI/Gg at different pH and ratios is presented in Fig. 1. As shown in Fig. 1A, the turbidity of the Gg solution remained constant at very low values in the pH 2–10 range, indicating that Gg did not form any aggregates. However, as the pH value decreased, the turbidity of the pcRPI solution changed and reached the maximum around its isoelectric point (pH 5.6). For pcRPI/Gg, during acid titration, four notable changes in the turbidity values were also observed: pH_c, $pH_{\varphi1}$, pH_{max} and $pH_{\varphi2}$ (Fig. 1B). pH_c is the pH value at which the slope of the turbidity curve initially changes; $pH_{\varphi1}$ is the pH value at which a sudden increase in the turbidity curve's slope occurs; pH_{max} represents the pH value at which the turbidity reaches its maximum, and $pH_{\varphi2}$ denotes the pH value corresponding to the point where the slope of the turbidity curve decreases to a stable level.[32] These critical boundary pH values also correspond to distinct phase behaviors:[33] (i) cosoluble polymer (at $pH > pH_c$): pcRPI and Gg both carried negative charges, and due to electrostatic repulsion, each remained stable in a monomeric form, thereby preventing the formation of coacervates; (ii) soluble complex (at $pH_{\varphi1} < pH < pH_c$): the turbidity of the composite solution started to increase, suggesting that protein and Gg formed soluble complexes with the ability to scatter light in the solution; (iii) complex coacervates (at $pH_{\varphi2} < pH < pH_{\varphi1}$): the emergence of insoluble composite

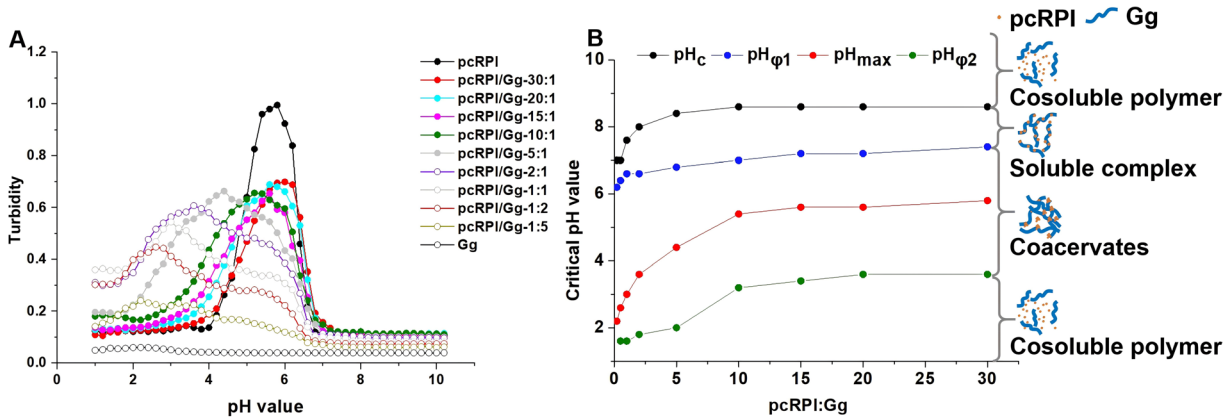

Fig. 1 Effect of pH and mass ratio on the turbidity of the pcRPI/Gg mixtures. (A) Turbidimetric titration curve and (B) state diagram of the pcRPI/Gg mixtures.

aggregates induced a macroscopic phase separation in the system; (iv) return to cosoluble polymer (pH < $pH_{\varphi 2}$): as the pH value decreased, the composite aggregates gradually dissociated, resulting in a reduction in turbidity. When the pH value exceeded the isoelectric point of pcRPI, although the protein carried a negative charge, the formation of soluble complexes with anionic polysaccharides was still feasible due to the weak electrostatic interactions. Similar phenomena were observed for ovalbumin/chondroitin sulfate[31] and rice bran protein/flaxseed gum[34] systems during the acidification process.

The ratio of proteins to polysaccharides influences the charge balance, subsequently altering the critical pH of the phase transition. As illustrated in Fig. 1, with the increase in the pcRPI/Gg mass ratio (from 1 : 5 to 30 : 1), the turbidity profile of the pcRPI/Gg system progressively approached a normal distribution, with the critical pH shifting towards higher values (Fig. 1B). As the proportion of Gg in the system increased, the absorption peak of the pcRPI/Gg mixture broadened, and the maximum absorption peak intensity gradually decreased. A similar phenomenon was observed in the study of composite coagulation involving tragacanth gum with pea protein isolate[35] and whey protein isolate with hyaluronic acid.[36] At a protein-to-polysaccharide ratio of 1 : 5, the turbidity of the composite solution was notably lower, indicating that the protein molecules were able to bind to the polysaccharide chains, which further inhibited interactions between the protein molecules. For the mixture of pcRPI/Gg, when the pcRPI : Gg ratio gradually increased, an elevated Gg fraction augmented the binding of negative charges on the pcRPI surface, thereby promoting the complex formation to a certain extent. Compared with that of the sole pcRPI, the pH_{max} of pcRPI/Gg decreased. This effect can be attributed to the intensified electrostatic repulsion from abundant sulfate and carboxyl groups on free polysaccharides, which constrain the protein/polysaccharide association and aggregate growth.[37] Generally, a certain total biopolymer content and ratio ranges promote phase separation or coacervation, while extremely high concentrations can increase viscosity and slow down or prevent phase separation. At a pcRPI : Gg ratio of 10 : 1, the pH_c, pH_φ and pH_{max} reached a relatively high level and remained stable with an increase in the protein content. It was considered that the Gg chain was saturated and adsorbed by pcRPI, and the amount of coacervates reached the maximum. Ratios above or below 10 : 1 lead to excess unbound protein or polysaccharide, respectively, resulting in weaker and less stable complexes.[38] A similar phenomenon was also reported for bovine serum albumin/sodium alginate[39] and scallop female gonad protein isolates/sodium alginate.[40] Many studies have also determined mass ratios through turbidity data, including for fish gelatin/*Tremella* polysaccharides[41] and scallop male gonad hydrolysates/Gg systems.[42] Therefore, the differences in the properties of the pcRPI/Gg composite gels in a mass ratio of 10 : 1 in the coacervate (pH 6), soluble complex (pH 8) and cosoluble polymer (pH 10) regions were further analyzed, while the potential impacts of mass ratios on pcRPI/Gg gelation will be analyzed in the future studies.

3.2 The visual appearance and rheological characteristics of pcRPI/Gg gels

As illustrated in Fig. 2, pcRPI/Gg presented as viscoelastic fluids after heat treatment at pH 10, and it showed gel behavior at pH 6 and 8. The sole pcRPI and Gg still existed in a fluid state after

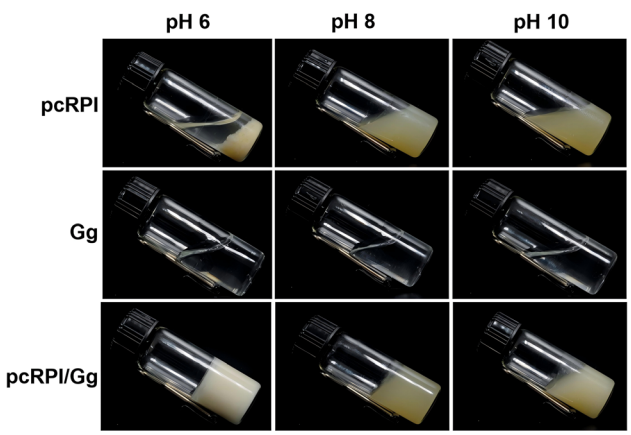

Fig. 2 The visual appearances of pcRPI, Gg and pcRPI/Gg gels at various pH levels.

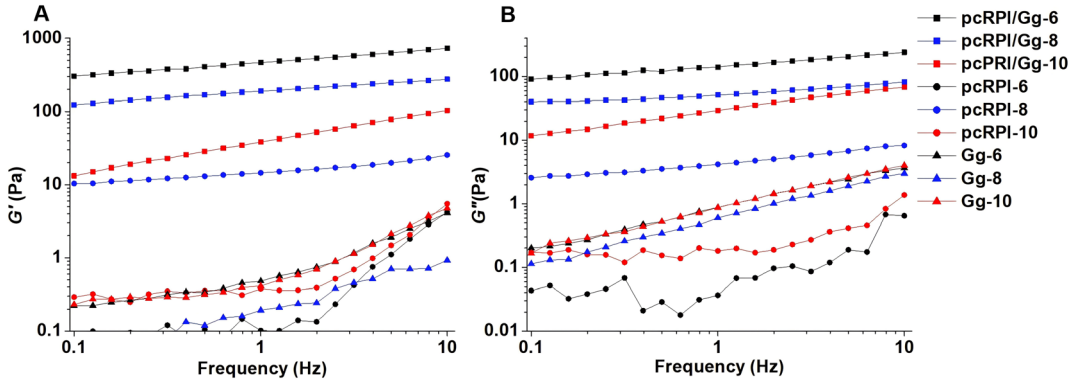

Fig. 3 The storage modulus G' (A) and loss modulus G'' (B) of pcRPI, Gg and pcRPI/Gg gels against frequency at various pH levels.

heat treatment at pH 6–10, and pcRPI exhibited significant insoluble protein precipitation at pH 6, as this value is near its isoelectric point. Therefore, the formation of a cosoluble polymer not only changed the solubility of pcRPI but also promoted the formation of heat-induced protein gels.

Furthermore, the rheological characteristics of different systems were analyzed. Initially, we investigated the influence of mass ratio (30 : 1 to 5 : 1) on the rheological properties of pcRPI/Gg hydrogels with a total biopolymer concentration of 55 mg mL^{-1}. The results showed that as the proportion of Gg increased, the G' values of the composite gel gradually increased (Fig. S1). Furthermore, upon reaching a ratio of 10 : 1, the G' of the pcRPI/Gg composite gels exceeded 200 Pa, indicating the formation of a stable gel structure. At 1 Hz, the G' value of pcRPI/Gg gels was about 15-fold and 1150-fold higher than those of Gg alone, which were approximately 55 Pa (9.2 mg mL^{-1}) and 0.5 Pa (5 mg mL^{-1}) at mass ratios of 5 : 1 and 10 : 1, respectively. This result indicated that a more pronounced interaction occurred between the pcRPI and Gg at 10 : 1. Moreover, the phase-separation behavior caused by pH and its impact on the properties of the composite gel were further investigated. As shown in Fig. 3, all pcRPI/Gg mixtures showed gel-like behaviors in the coacervate (pH 6), soluble complex (pH 8) and cosoluble polymer (pH 10) regions with higher G' values than those of the sole protein gels. When the pH increased, the G' values of pcRPI/Gg decreased. The G' values of the sole pcRPI gels were both <20 Pa, highlighting their soft-solid or viscoelastic-solid behavior. This phenomenon likely occurred because the protein concentration (55 mg mL^{-1}) was lower than the pcRPI gelation concentration, resulting in limited stretching and relaxation of the existing bonds within the pcRPI molecules.[43] Our previous study found that pcRPI can form gels at a concentration of 100 mg mL^{-1} and pH 7–9 after being heated at 85 °C for 20 min, while it could not form heat-induced gels at pH 6.[44] However, pcRPI/Gg formed gels at pH 6 and showed the highest G' value of 464.2 Pa at 1 Hz, which was 2.5-fold and 12.1-fold higher than those at pH 8 and pH 10, respectively. The isoelectric point of pcRPI is around pH 5.6;[12] thus, when the system pH exceeds the isoelectric point, both pcRPI and Gg will possess a net negative charge, reducing the likelihood of electrostatic attraction between the polymers.[45] Accordingly, as the pH decreased, the G' and G'' values of the pcRPI/Gg complex system increased, enhancing the electrostatic attraction between the two biopolymers. This result indicated the formation of a highly interconnected gel-like network with pronounced elastic characteristics, which is likely governed primarily by electrostatic interactions between the protein molecules and polysaccharide chains.[46] At pH 6.0, it is likely that large aggregates of insoluble pcRPI/Gg complexes generated stronger fluid resistance compared to the cosolubility observed at pH 8.0 and pH 10.0. Such behaviors have been reported in other systems, such as soy protein/polysaccharide[47] and scallop male gonad hydrolysates/sodium alginate complex coacervate systems.[48] In addition, the power-law model was employed to describe the relationship between the modulus and frequency of the non-Newtonian system. The n' and n''

Table 1 The power-law model parameters of large yellow croaker (*Pseudosciaena crocea*) roe protein isolate/gellan gum gels[a]

Sample	k' (Pa s^{-n})	n'	k'' (Pa s^{-n})	n''
pcRPI/Gg-pH 6	151.74 ± 21.79^{a}	0.17 ± 0.01^{d}	47.18 ± 0.75^{a}	0.21 ± 0.02^{c}
pcRPI/Gg-pH 8	137.97 ± 0.02^{a}	0.17 ± 0.00^{d}	38.36 ± 0.49^{b}	0.17 ± 0.01^{c}
pcRPI/Gg-pH 10	23.61 ± 8.98^{b}	0.42 ± 0.03^{cd}	17.69 ± 4.35^{c}	0.38 ± 0.001^{c}
pcRPI-pH 6	0.001 ± 0.00^{c}	1.98 ± 0.08^{a}	0.003 ± 0.002^{e}	1.37 ± 0.25^{a}
pcRPI-pH 8	14.52 ± 4.92^{bc}	0.12 ± 0.09^{d}	3.21 ± 0.62^{d}	0.25 ± 0.02^{c}
pcRPI-pH 10	0.02 ± 0.02^{c}	1.33 ± 0.67^{abc}	0.01 ± 0.00^{e}	1.19 ± 0.01^{a}
Gg-pH 6	0.06 ± 0.04^{c}	1.13 ± 0.30^{abc}	0.28 ± 0.03^{e}	0.62 ± 0.01^{b}
Gg-pH 8	0.03 ± 0.04^{c}	1.46 ± 1.13^{ab}	0.15 ± 0.01^{e}	0.72 ± 0.02^{b}
Gg-pH 10	0.22 ± 0.26^{c}	0.71 ± 0.60^{bcd}	0.31 ± 0.07^{e}	0.63 ± 0.06^{b}

[a] Data are expressed as means ± SD from triplicate determinations. Different letters in the same column indicate significant differences ($P < 0.05$).

values represent the frequency dependence of different gels, whereas the k' and k'' values are associated with the gel's properties.[49] As shown in Table 1, both k' and k'' values of the composite gels were higher than those of the individual protein or polysaccharide systems, indicating a denser cross-linked network that enhanced the elasticity and structural stability of the gels. Moreover, as the pH decreased, the k' and k'' values of pcRPI/Gg slightly increased. The pcRPI/Gg gels also exhibited relatively low n' values (0.17–0.42), reflecting weak frequency dependence and implying that their viscoelastic response was less affected by the applied oscillatory frequency. Therefore, the complex coacervation of pcRPI with Gg improved the gel strength of pcRPI in different phases and enabled pcRPI to form a gel near the isoelectric point.

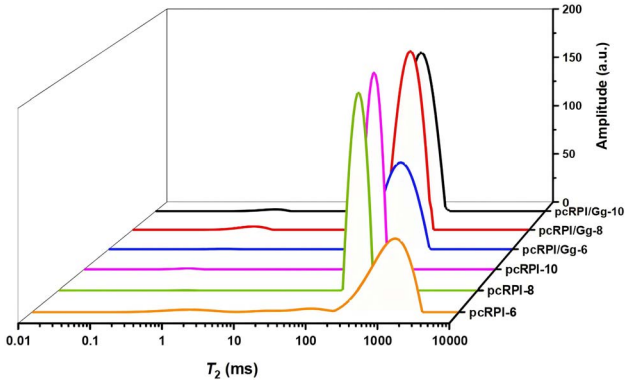

Fig. 4 The relaxation time T_2 curves of pcRPI and pcRPI/Gg gels at various pH levels.

3.3 The textural properties of pcRPI/Gg gels

In addition, TPA was conducted to discuss the hardness, springiness, cohesiveness, chewiness and gumminess of the pcRPI/Gg gels. Among the parameters, hardness is the force required for the gel to achieve the target deformation, chewiness is the energy required for the gel to reach the swallowing state, and springiness is the ability of a material to stretch and return to its original length.[50] Due to the flow or weak gel state of sole pcRPI and Gg, they could not be accurately detected by TPA. As shown in Table 2. With the increase in pH, the hardness of the gel decreased significantly from 57.15 to 45.87, corresponding to the rheological results (Fig. 3). The cohesiveness of the pcRPI/Gg gel increased with the pH, while different pH values had little effect on the elasticity of the pcRPI/Gg gel. The springiness values of all pcRPI/Gg gels were more than 0.94, which further proves that the pcRPI/Gg gels were more inclined to be elastic gels.[51] In this study, although the purity of pcRPI was 80.5%, the pcRPI/Gg systems could form heat-induced gels at 55 mg mL^{-1}. These results suggested that the pcRPI/Gg gel systems have great potential for applications in food fields and other functional materials, and their application value can be further elevated by improving their purity in future studies.

3.4 Effect of pH on relaxation time T_2 of the pcRPI/Gg gels

LF-NMR is frequently used for analyzing the water distribution in food products, particularly gels, and it is non-destructive and highly sensitive as regards capturing subtle changes in water mobility.[52] Fig. 4 illustrates the distribution of the T_2 relaxation times for the pcRPI/Gg gels at different pH levels, displaying two distinct peaks centered at 0.9–2.9 ms (T_{21}) and 130.1–208.1 ms (T_{23}). Generally, T_{21} indicates bound water that interacts closely with macromolecules *via* non-covalent bonds, including electrostatic interactions, hydrogen bonding, and hydrophobic forces. In contrast, T_{23} corresponds to free water, which exists outside the gel network and displays unrestricted mobility.[53] Most of the moisture in Gg (5 mg mL^{-1}) is free water at different pH values, with T_{23} values exceeding 1700 ms (data not shown). Previous studies have also found that the T_{23} values of Gg at 2–10 mg mL^{-1} are about 1431–2035 ms.[42,54,55] Moreover, T_{21} occupied a minor part in different pcRPI/Gg complexes and was almost not affected by pH and Gg addition. The addition of Gg led to a shift of the pcRPI T_{23} toward shorter times, while it did not change significantly compared with that of pcRPI, except at pH 6 (Table 3). Ge *et al.*[56] also reported that the T_{23} values of a set of yoghurts mixed with Gg did not change significantly. The shorter relaxation times indicate a stronger interaction between water and the biopolymer.[25] The incorporation of Gg facilitated the development of a gel structure at pH 6, which may have immobilized the outer hydration layer, thereby shortening T_{23}. This decreasing trend was related to the water uptake of gels, suggesting an enhanced binding effect of the gel to water with Gg addition. Moreover, there was an additional peak for pcRPI-6 at 79.1 ± 18.7 ms (data not shown), which may be attributed to the insoluble protein particles bound to the water molecules; notably, this peak was not observed for pcRPI/Gg-6. Additionally, as the pH increased, the T_{23} values of pcRPI and pcRPI/Gg gels shifted slightly toward shorter times, revealing an increased water-binding ability and restricted water movement at higher pH values, similar to the observations in our previous study.[44] These results suggested that the addition of Gg had a slight effect on the migration rate of water molecules in the co-soluble state of the pcRPI complexes, whereas it promoted water interception in the coacervate state.

Table 2 Texture profile analysis of large yellow croaker (*Pseudosciaena crocea*) roe protein isolate/gellan gum gels[a]

Sample	Hardness (g)	Springiness	Cohesiveness	Chewiness (g)	Gumminess (g)
pcRPI/Gg-pH 6	57.15 ± 7.57^{a}	0.95 ± 0.01^{a}	0.79 ± 0.03^{b}	42.91 ± 7.13^{ab}	45.24 ± 7.28^{ab}
pcRPI/Gg-pH 8	47.37 ± 5.34^{b}	0.94 ± 0.01^{a}	0.83 ± 0.03^{b}	36.91 ± 3.15^{b}	39.15 ± 3.26^{b}
pcRPI/Gg-pH 10	45.87 ± 2.52^{b}	0.96 ± 0.02^{a}	1.05 ± 0.04^{a}	46.44 ± 4.13^{a}	48.33 ± 4.31^{a}

[a] Data are expressed as means ± SD from triplicate determinations. Different letters in the same column indicate significant differences ($P < 0.05$).

Table 3 The LF-NMR parameters of large yellow croaker (*Pseudosciaena crocea*) roe protein isolate/gellan gum gels[a]

Sample	Relaxation time (ms)	
	T_{21} (ms)	T_{23} (ms)
pcRPI/Gg-pH 6	1.63 ± 1.20^{ab}	208.05 ± 11.97^{b}
pcRPI/Gg-pH 8	2.93 ± 1.28^{ab}	157.45 ± 4.99^{b}
pcRPI/Gg-pH 10	0.94 ± 0.35^{b}	130.10 ± 9.09^{b}
pcRPI-pH 6	3.68 ± 1.99^{a}	1549.16 ± 414.01^{a}
pcRPI-pH 8	2.30 ± 0.87^{ab}	201.66 ± 4.59^{b}
pcRPI-pH 10	2.21 ± 1.41^{ab}	172.36 ± 8.46^{b}

[a] Data are expressed as means ± SD from triplicate determinations. Different letters in the same column indicate significant differences ($P < 0.05$).

3.5 Effect of pH on the microstructure of the pcRPI/Gg complex

Cryo-SEM is frequently utilized for analyzing the microstructure of food products, and it offers high-resolution imaging capabilities, allowing for the observation of delicate structures and the spatial distribution of samples.[57] In Fig. 5, pcRPI/Gg shows a heterogeneous network structure with uniform holes, while pcRPI at pH 6/10 and Gg at pH 6–10 did not show a gel network structure. In detail, protein aggregates appeared at pH 6 due to poor solubility near the isoelectric point of the pcRPI, and the microstructure of Gg at pH 8–10 was similar to that of a thin film. Gg at pH 6 showed a large and broken mesh structure, and the wall of the structure was relatively thin and contained numerous small cavities. Nie *et al.*[58] also found that pure Gg shows a uniform structure with large pores. Moreover, the electrostatic interaction between Gg and pcRPI prevented the precipitation of proteins and facilitated the development of a three-dimensional gel network structure. Several studies have also indicated that the incorporation of Gg improves the microstructural properties of protein gels, including oat protein isolate,[59] egg white proteins[60] and soy protein isolate.[61] Furthermore, the cryo-SEM images of samples were analyzed using the AngioTool software, including VPA, TNJ and lacunarity. The AngioTool software was originally developed for the microscopic analysis of vascular networks in medical research. Currently, it has been widely applied in the analysis of microstructures of various materials.[62] Fig. 5 shows the network parameters of the pcRPI/Gg gels at various pH values. The VPA and TNJ of pcRPI/Gg-pH 6 are significantly higher than those of other pcRPI/Gg gels, while the lacunarity is significantly lower than those of other pcRPI/Gg gels ($p < 0.05$). Networks with a uniform organization and consistent pore sizes exhibit low lacunarity, whereas the presence of irregular gaps and large voids increases lacunarity.[62] These results indicated that as pH decreased, the pcRPI/Gg gel exhibited a denser structure. Generally, pore size is related to the interactions between protein and polysaccharide molecules; smaller pore sizes correspond to greater gel strength, consistent with our

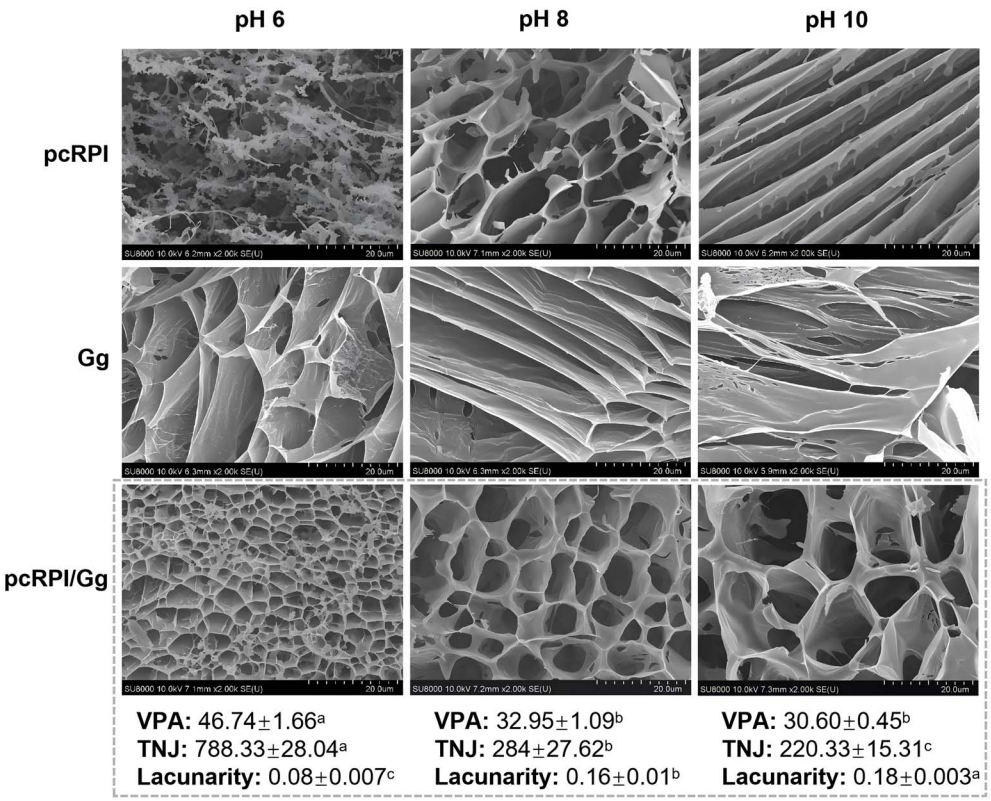

Fig. 5 The cryo-SEM micrographs of pcRPI, Gg and pcRPI/Gg gels at various pH levels. The vessel percentage area (VPA), total number of junctions (TNJ) and lacunarity of cryo-SEM images analyzed by the AngioTool software. Different letters (a–c) indicate significant differences in the VPA, TNJ and lacunarity ($p < 0.05$) for the different samples.

rheological data (Fig. 3). A previous study has also shown that as the pH decreases, the hole sizes of scallop male gonad protein hydrolysates/κ-carrageenan complexes decrease with higher G' values.[25] Therefore, it is suggested that Gg facilitated the formation of a uniform three-dimensional network structure of pcRPI at different pH environments and transformed the aggregated state of pcRPI near its isoelectric point into a more compact and continuous network structure.

3.6 Correlation analysis

The relationships among the G' values at 1 Hz, textural properties, and microstructural parameters of the pcRPI/Gg gels were further examined by correlation analysis. As shown in Fig. 6, the G' exhibited positive correlations with hardness, VPA and TNJ, with correlation coefficients of 0.70, 0.71 and 0.68, respectively, indicating that enhanced viscoelastic behavior was associated with improved gel strength and network connectivity. Meanwhile, hardness, VPA and TNJ were perfectly correlated with each other ($r = 1.00$), demonstrating a strongly positive correlation among these parameters. In contrast, lacunarity showed strong negative correlations with G', hardness, VPA and TNJ, with correlation coefficients of −0.75, −1.00, −1.00 and −1.00, respectively. This suggests that a lower lacunarity, corresponding to fewer and more uniformly distributed pores, is closely related to a more homogeneous microstructure and better mechanical properties. Overall, these correlations indicate that the incorporation of Gg promotes the formation of a denser and more uniform network in pcRPI gels, thereby enhancing the gel properties.

3.7 Molecular docking and MD simulation study

To further elucidate the interaction mechanism between pcRPI and Gg under different pH conditions, molecular docking and molecular dynamics simulations were performed. Our previous study revealed that the primary protein component in pcRPI is vitellogenin.[12] Therefore, vitellogenin can be used as a representative protein to investigate protein interactions with Gg. The protein–ligand complexes were visualized using Pymol 2.1 for further analysis. In this study, the Gg was docked with the vitellogenin at pH levels of 6, 8, and 10. The molecular docking results indicated that vitellogenin exhibited strong binding affinity and high compatibility with the Gg, and the binding energies were −9.42, −9.12 and −8.71 kcal mol^{-1} at pH 6, 8 and 10, respectively. Furthermore, the complexes were visualized to reveal the binding mode between protein and Gg. As shown in Fig. 7, at pH 6, eight amino acid residues (Asp 186, Cys 188, Arg 191, Asp 195, Thr 201, His 203, Gln 208, and Arg 790) bind with Gg by conventional hydrogen bonds, two amino acid residues (Ala 671 and Ser 803) by carbon hydrogen bonds, and one amino acid residue (Leu 802) by hydrophobic interactions. At pH 8, eight amino acid residues (Asp 195, Thr 201, His 203, Lys 212, Asp 449, Lys 528, Asp 449, and Arg 790) bind with Gg by conventional hydrogen bonds, one amino acid residue (Ile 448) by carbon hydrogen bonds, and one amino acid residue (Ala 451) by hydrophobic interactions. At pH 10, six amino acid residues (Glu 190, Arg 191, Met 193, Lys 212, Leu 214, and Asp 449) bind with Gg by conventional hydrogen bonds and two amino acid residues (Asp 186 and Gln 208) by carbon–hydrogen bonds. Thus, hydrogen bonds are essential for stabilizing the molecule within the protein cavity, and hydrophobic interactions further contribute to the stability of the complexes. Variations in the binding sites of vitellogenin may be due to changes in its positive charge distribution. At pH levels above the isoelectric point, a strong repulsion occurred between the protein and Gg. A similar phenomenon was observed regarding the binding sites between bovine serum albumin and sodium alginate.[63]

Moreover, the correlation between the electrostatic potential of the binding pocket and the docking scores was further analyzed. As shown in Fig. 8A, the binding pocket of vitellogenin exhibited a strong positive potential (blue-colored surface) at pH 6. This positive environment was highly complementary to the anionic nature of Gg, which was rich in deprotonated carboxylate groups, thus facilitating strong electrostatic attraction and leading to the most favorable binding energy (−9.42 kcal mol^{-1}). As the pH increased to 8 and 10, key residues within the pocket (*e.g.*, His 203, Lys 212, and Lys 528) were deprotonated. This resulted in a progressive decrease in the positive charge of the binding pocket, which transitioned toward a more neutral or even slightly negative potential (Fig. 8B and C). The diminished electrostatic complementarity accounted for the observed decline in the binding affinity, with binding energies decreasing to −9.12 kcal mol^{-1} at pH 8 and −8.71 kcal mol^{-1} at pH 10. This trend is also consistent with the turbidity change in pcRPI/Gg (Fig. 1). At pH 6, the system exhibited maximal turbidity, indicative of complex coacervate formation. As the pH increased, the complexes progressively dissociated, and the suspension became clear with low turbidity. Molecular docking also showed that positively charged surface patches in the protein binding pocket enhance electrostatic complementarity and promote tight association with anionic Gg. Deprotonation at higher pH levels removes these positive patches and thus weakens the protein–

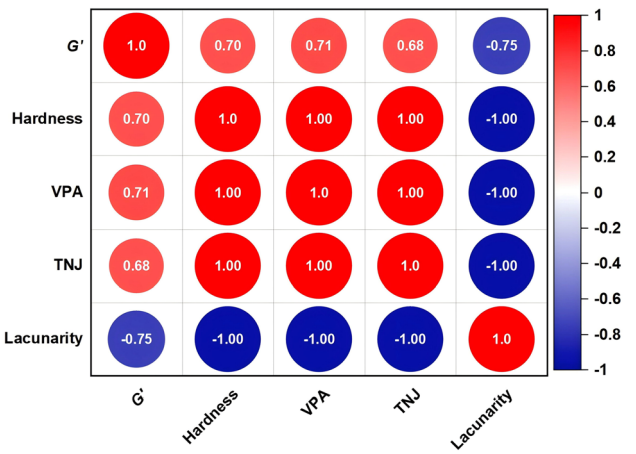

Fig. 6 Correlation analysis of the gel properties and microstructural characteristics of pcRPI/Gg gels at various pH levels. Positive correlation is represented by red and negative correlation by blue.

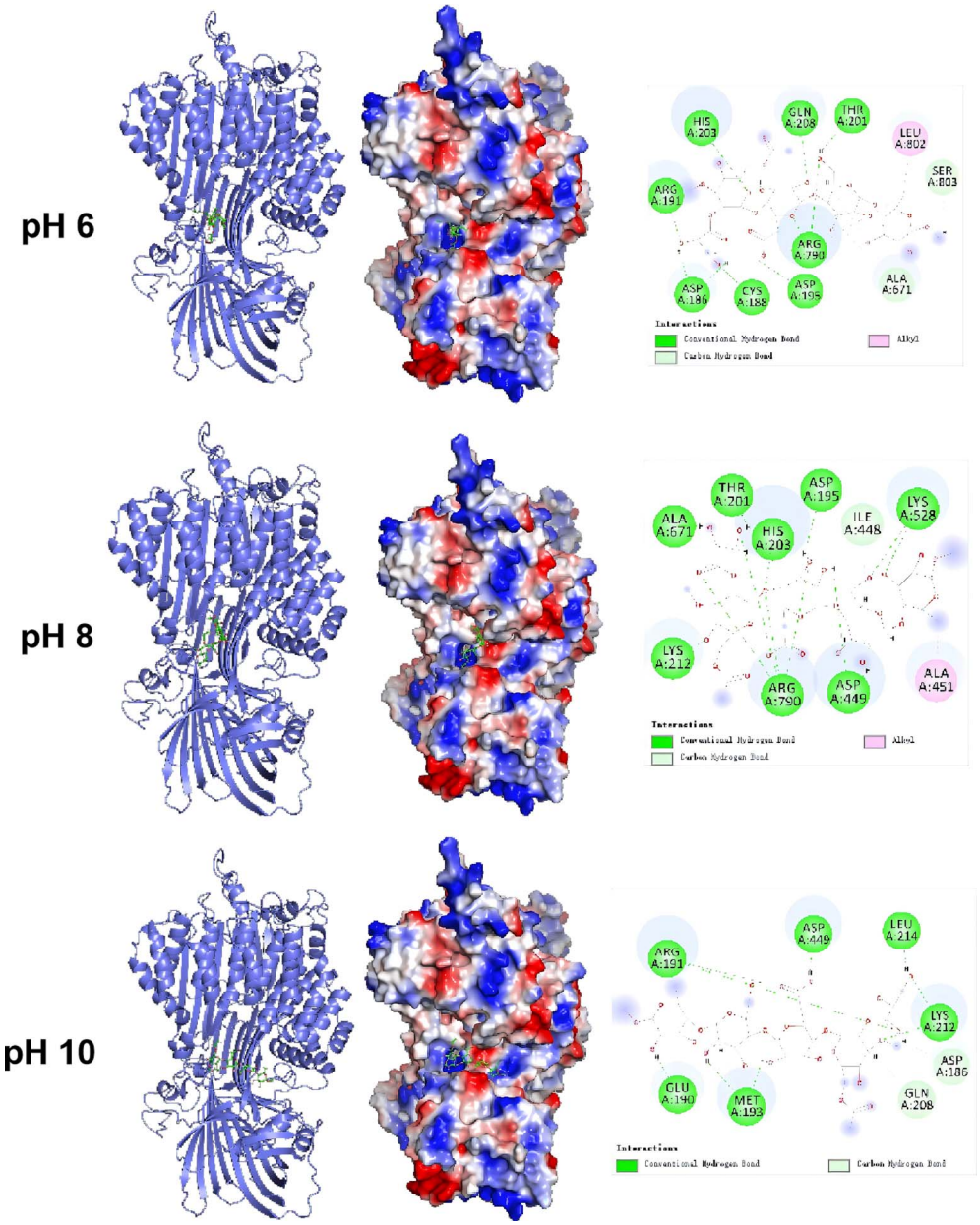

Fig. 7 The 3D docking model and 2D schematic of the interaction between vitellogenin and Gg at various pH levels.

polysaccharide interaction. Moreover, the pcRPI/Gg complexes exhibited the largest binding energy magnitude at pH 6, highlighting the strong interaction between both components; further, they showed better gelation performance with higher G' values and superior water-retention capacity (Fig. 3 and 4). To gain deeper insights into Gg–protein interactions, a 100 ns molecular dynamics simulation on the protein–Gg complexes was conducted. As shown in Fig. 9A, the average RMSD of vitellogenin is less than 8.0 Å, and the complex reached equilibrium after about 20 ns, suggesting good compatibility between the Gg and the vitellogenin, enabling the formation of a stable complex. Additionally, there were no significant discontinuities in the conformational changes of the complex, indicating that Gg binds well to the protein without leaving the active pocket. Furthermore, the RMSD fluctuations for the vitellogenin/Gg complex formed at pH 6 were notably smaller than those for the other two complexes, suggesting that it is more stable than the others. Root mean square fluctuation was used to characterize the conformational changes in each amino acid in the protein chain during the simulation (Fig. 9B). Peaks represent regions with the highest fluctuations in amino acids. A larger RMSF value indicates greater conformational flexibility of the amino acid residue. According to Fig. 9B, a small portion of amino acids in the vitellogenin/Gg complexes exhibited large conformational changes (*e.g.*, around the 700–1000 region), likely because these amino acids are located in the β-sheet region of the protein, which is relatively isolated and lacks

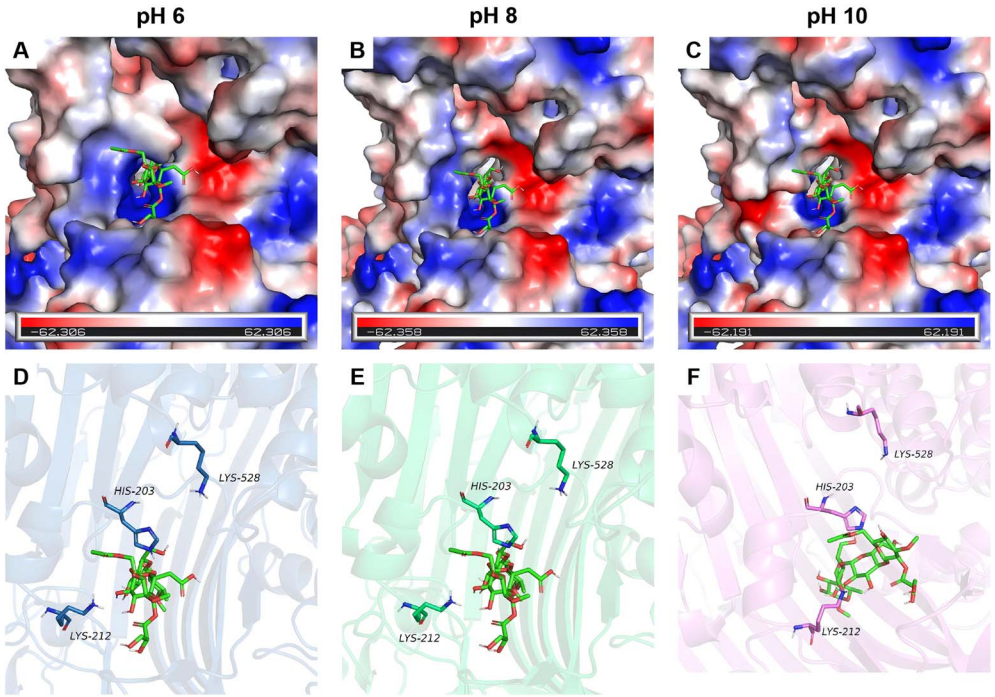

Fig. 8 Influence of pH on the electrostatic potential and protonation states of the key residues in the binding site (A–C). The electrostatic potential surface of the binding pocket at pH 6.0 (A), 8.0 (B), and 10.0 (C). The surface is colored according to the electrostatic potential, ranging from red (−62*kT*/*e*) to blue (+62*kT*/*e*). (D–F) Detailed view of the protonation states of the key active site residues at the corresponding pH values of 6.0 (D), 8.0 (E), and 10.0 (F).

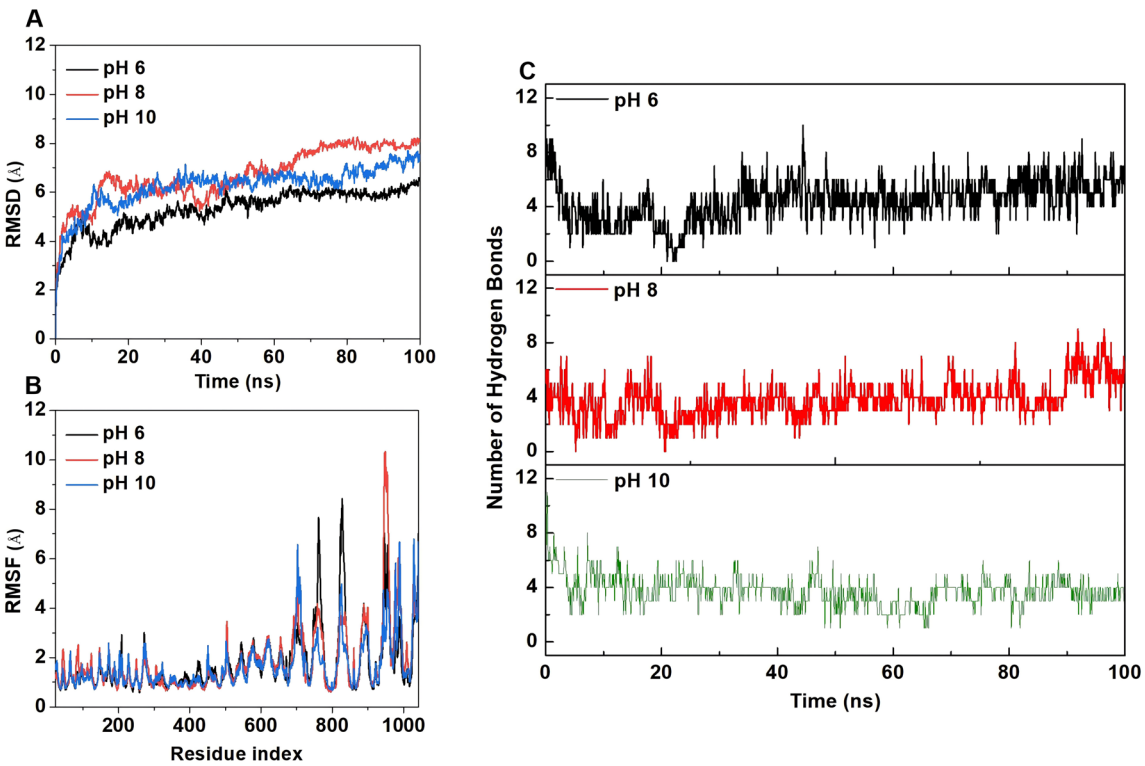

Fig. 9 RMSD during molecular dynamics simulations for the complexes (A). RMSF during molecular dynamics simulations for the complexes (B). The hydrogen bond number changes during the molecular dynamics study (C).

effective interactions with surrounding residues, making the conformations more prone to change during the simulation.

Fig. 9C shows the number of hydrogen bonds between vitellogenin and Gg as a function of the simulation time. It is clear that the Gg could form around four hydrogen bonds with the protein pocket amino acids for the majority of the simulation time, playing a crucial role in stabilizing the complexes. Among the three complexes, vitellogenin/Gg-pH 6 formed slightly more hydrogen bonds than the other two. The number of hydrogen bonds showed a negative correlation with the ligand RMSD value (Fig. 9A), suggesting that hydrogen bonds positively influence the complex stability. Furthermore, the findings revealed that at pH 6, the vitellogenin/Gg complex exhibited relatively high binding capacity and stability. Liu *et al.*[64] also found that compared to the results at pH 2, 4, and 7, β-lactoglobulin–sodium alginate complex exhibited a relatively high binding capacity and stability at pH 5 with lower RMSD values and a higher number of hydrogen bonds. Overall, these results indicated that a stable vitellogenin/Gg complex was formed during the MD simulation due to favorable interactions at pH 6.0, which may also contribute to the composite gel formation.

4 Conclusions

In conclusion, the formation of soluble and insoluble complexes between pcRPI with Gg is dependent on the pH and protein to polysaccharide ratio. The pcRPI/Gg gels showed a higher G' value in the insoluble coacervate phase (pH 6). The addition of Gg also improved the gel strength of the pcRPI gel in different phases, especially at pH 6, where the protein alone failed to form a gel, but the addition of Gg resulted in a dense network structure. Meanwhile, the pcRPI/Gg gels showed denser network microstructures with smaller pore sizes at acidic pH levels. At pH 6, the greater number of hydrogen bonds formed between pcRPI and Gg contributed to the enhanced stability of the complex, potentially promoting gel formation and resulting in better gelation properties. Therefore, pcRPI/Gg gels show a wide application range, and they can be regulated to exhibit excellent rheological properties and microstructures by adjusting the pH and mass ratios. The binary gels also exhibit great application potential in the food and biological materials fields, particularly for applications such as texture modification and nutrient microencapsulation.

Conflicts of interest

There are no conflicts to declare.

Abbreviations

pcRPI	*Pseudosciaena crocea* roe protein isolates
Gg	Gellan gum
G'	Storage modulus
G''	Loss modulus
LF-NMR	Low-field nuclear magnetic resonance
Cryo-SEM	Cryo-scanning electron microscopy
VPA	Vessel percentage area
TNJ	Total number of junctions
MD	Molecular dynamics
RMSD	Root mean square deviation
RMSF	Root mean square fluctuation
TPA	Texture profile analysis

Data availability

The data are available on request.

Supplementary information (SI): rheological properties of pcRPI/Gg gels at different mass ratios. See DOI: https://doi.org/10.1039/d5fb00392j.

Acknowledgements

This work was supported by the National Key R&D Program of China (2023YFD2100805), the Liaoning Province Science and Technology Plan United Program (2025-BSLH-040), and the Scientific Research Project for Introducing Talents of Dalian Polytechnic University (LJBKY2025064).

References

1 C. J. F. Souza and E. E. Garcia-Rojas, Interpolymeric complexing between egg white proteins and xanthan gum: Effect of salt and protein/polysaccharide ratio, *Food Hydrocolloids*, 2017, **66**, 268–275.
2 V. Sarabi-Aghdam, S. H. Hosseini-Parvar, A. Motamedzadegan and S. M. Razi, Phase behavior and rheological properties of basil seed gum/whey protein isolate mixed dispersions and gels, *Food Sci. Nutr.*, 2021, **9**, 1881–1895.
3 F. Meng, J. Li, C. Yang, M. Wang and X. Liu, Rheological and tribological properties of high internal phase emulsions stabilized by pH-induced soy protein isolate-carrageenan complex coacervates, *Food Hydrocolloids*, 2024, **146**, 109191.
4 Y. Xu, Y. Lv, Y. Yin, H. Zhao, X. Li, S. Yi and J. Li, Improvement of the gel properties and flavor adsorption capacity of fish myosin upon yeast β-glucan incorporation, *Food Chem.*, 2022, **397**, 133766.
5 X. Li, M. Fan, Q. Huang, S. Zhao, S. Xiong, T. Yin and B. Zhang, Effect of micro- and nano-starch on the gel properties, microstructure and water mobility of myofibrillar protein from grass carp, *Food Chem.*, 2022, **366**, 130579.
6 C. Cao, Y. Xu, B. Kong, X. Xia, Q. Chen, H. Zhang and Q. Liu, Changes of rheological behavior, thermal and microstructural properties of myofibrillar protein-κ-carrageenan mixed sol as mediated by NaCl concentration, *Food Biosci.*, 2023, **55**, 103035.
7 W. Xiong, C. Ren, W. Jin, J. Tian, Y. Wang, B. R. Shah, J. Li and B. Li, Ovalbumin-chitosan complex coacervation: Phase behavior, thermodynamic and rheological properties, *Food Hydrocolloids*, 2016, **61**, 895–902.
8 C. Schmitt, C. Sanchez, S. Desobry-Banon and J. Hardy, Structure and technofunctional properties of protein-

polysaccharide complexes: A review, *Crit. Rev. Food Sci. Nutr.*, 1998, **38**, 689–753.

9 X. Hu, Q. Ju, C. K. W. Koo and D. J. McClements, Influence of complex coacervation on the structure and texture of plant-based protein-polysaccharide composites, *Food Hydrocolloids*, 2024, **147**, 109333.

10 D. E. Igartúa, A. Balcone, F. A. Platania, D. M. Cabezas and G. G. Palazolo, Pea protein isolate–soluble soybean polysaccharides electrostatic assembly: effect of pH, biopolymer mass ratio and heat treatment, *J. Sci. Food Agric.*, 2024, **104**, 7291–7300.

11 J. Zhang, Y. Shi, Y. Hu, W. Fan, W. Liu and Y. Liu, Insight on the interaction between chickpea protein isolate and dextran: Structural analysis, functional characterization and co-encapsulated W/O/W emulsion formation, *Food Res. Int.*, 2025, **213**, 116593.

12 Y. N. Du, S. Xue, J. R. Han, J. N. Yan, W. H. Shang, J. N. Hong and H. T. Wu, Simultaneous extraction by acidic and saline solutions and characteristics of the lipids and proteins from large yellow croaker (*Pseudosciaena crocea*) roes, *Food Chem.*, 2020, **310**, 125928.

13 Y.-N. Du, J. Jia, J.-N. Yan, S.-Q. Xu, Y.-Q. Wang and H.-T. Wu, Non-covalent interactions between large yellow croaker (*Pseudosciaena crocea*) roe protein isolates and curcumin: Implications for enhanced curcumin delivery, *Food Biosci.*, 2024, **60**, 104270.

14 S. R. Monteiro and J. A. Lopes-da-Silva, Effect of the molecular weight of a neutral polysaccharide on soy protein gelation, *Food Res. Int.*, 2017, **102**, 14–24.

15 C. Wang, Y. Gong, Y. Lin, J. Shen and D.-A. Wang, A novel gellan gel-based microcarrier for anchorage-dependent cell delivery, *Acta Biomater.*, 2008, **4**, 1226–1234.

16 X. Yu, L. Chen, L. Li, X. Chen, X. Qiu, Q. Tu, H. Yang and M. Xiao, Influence of κ-carrageenan/gellan gum ratios on the capsule properties of enteric plant dropping pills, *Int. J. Biol. Macromol.*, 2025, **321**, 146285.

17 J. Ryu and D. J. McClements, Control of plant-based biopolymer composite gel texture: Combining potato proteins with different high acyl-low acyl gellan gum ratios, *Food Hydrocolloids*, 2024, **149**, 109636.

18 N. Guo, Y. Ma, F. Zhang, G. Zhu, Z. Yu, H. Dai and Z. Wang, Effect of pH on the thermal gel properties of whey protein isolate-high acyl gellan gum, *J. Sci. Food Agric.*, 2023, **103**, 3346–3352.

19 F. G. Silva, A. B. S. Passerini, L. Ozorio, C. S. F. Picone and F. A. Perrechil, Interactions between pea protein and gellan gum for the development of plant-based structures, *Int. J. Biol. Macromol.*, 2024, **255**, 128113.

20 M. Bian, G. Hou, Z. Tan, L. Zhang, S. Miao, B. Zheng and F. Zhou, 3D-printed ultra-sensitive strain sensors using biogels prepared from fish gelatin and gellan gum, *Carbohydr. Polym.*, 2025, **352**, 123200.

21 X. Liu, Z. Chen, Y. Ye, M. Qian, B. Ou, J. Wen, W. Bai and H. Jiang, Effects of exogenous substances on the characteristics of low-salt tilapia surimi gel, *Food Chem.*, 2025, **484**, 144453.

22 Z. Liu, C. Liu, X. Sun, S. Zhang, Y. Yuan, D. Wang and Y. Xu, Fabrication and characterization of cold-gelation whey protein-chitosan complex hydrogels for the controlled release of curcumin, *Food Hydrocolloids*, 2020, **103**, 105619.

23 J. Liu, J. Chai, Y. Yuan, X. Wu, L. Gong, P. Yu, P. Liu, T. Zhang and X. Shang, Designation and characterization of cold-set egg white protein/dextran sulfate hydrogel for curcumin entrapment, *Food Chem.*, 2023, **419**, 136038.

24 Y.-N. Du, J.-N. Yan, S.-Q. Xu, Y.-Q. Wang, X.-C. Wang and H.-T. Wu, Formation and characteristics of curcumin-loaded binary gels formed from large yellow croaker (*Pseudosciaena crocea*) roe protein isolate and gellan gum, *Food Chem.*, 2023, **405**, 134759.

25 J.-N. Yan, Y.-Q. Wang, X.-Y. Jiang, J.-R. Han, Y.-N. Du, J.-F. Pan and H.-T. Wu, Effect of pH and mixing ratio on interpolymer complexation of scallop (*Patinopecten yessoensis*) male gonad hydrolysates and κ-carrageenan, *Food Chem.*, 2021, **336**, 127687.

26 Y. N. Du, S. Q. Xu, Y. Q. Wang, X. C. Wang and H. T. Wu, Fabrication and characterization of cold-set large yellow croaker (*Pseudosciaena crocea*) roe protein isolate gels, *LWT–Food Sci. Technol.*, 2022, **158**, 113135.

27 J.-N. Yan, W.-H. Shang, J. Zhao, J.-R. Han, W.-G. Jin, H.-T. Wang, Y.-N. Du, H.-T. Wu, S. Janaswamy and Y. L. Xiong, Gelation and microstructural properties of protein hydrolysates from trypsin-treated male gonad of scallop (*Patinopecten yessoensis*) modified by κ-Carrageenan/K^+, *Food Hydrocolloids*, 2019, **91**, 182–189.

28 M. Rajeswari, N. Santhi and V. Bhuvaneswari, Pharmacophore and Virtual Screening of JAK3 inhibitors, *Bioinformation*, 2014, **10**, 157–163.

29 R. Fazi, C. Tintori, A. Brai, L. Botta, M. Selvaraj, A. Garbelli, G. Maga and M. Botta, Homology Model-Based Virtual Screening for the Identification of Human Helicase DDX3 Inhibitors, *J. Chem. Inf. Model.*, 2015, **55**, 2443–2454.

30 V. Umashankar, S. H. Deshpande, H. V. Hegde, I. Singh and D. Chattopadhyay, Phytochemical moieties from Indian traditional medicine for targeting dual hotspots on SARS-CoV-2 spike protein: An integrative *in-silico* approach, *Front. Med.*, 2021, **8**, 672629.

31 J. Liu, J. Chai, T. Zhang, Y. Yuan, R. K. Saini, M. Xu, S. Li and X. Shang, Phase behavior, thermodynamic and rheological properties of ovalbumin/dextran sulfate: Effect of biopolymer ratio and salt concentration, *Food Hydrocolloids*, 2021, **118**, 106777.

32 M. Ghobadi, A. Koocheki, M. J. Varidi and M. Varidi, Fabrication and characterization of Grass pea (*Lathyrus sativus*) protein isolate-*Alyssum homolocarpum* seed gum complex coacervate, *Polym. Test.*, 2020, **89**, 106636.

33 E. A. Cortés-Morales, G. Mendez-Montealvo and G. Velazquez, Interactions of the molecular assembly of polysaccharide-protein systems as encapsulation materials. A review, *Adv. Colloid Interface Sci.*, 2021, **295**, 102398.

34 E. Hasanvand, A. Rafe and B. Emadzadeh, Phase separation behavior of flaxseed gum and rice bran protein complex coacervates, *Food Hydrocolloids*, 2018, **82**, 412–423.

35 J. Carpentier, E. Conforto, C. Chaigneau, J.-E. Vendeville and T. Maugard, Complex coacervation of pea protein isolate and tragacanth gum: Comparative study with commercial polysaccharides, *Innovative Food Sci. Emerging Technol.*, 2021, **69**, 102641.
36 W. Zhong, C. Li, M. Diao, M. Yan, C. Wang and T. Zhang, Characterization of interactions between whey protein isolate and hyaluronic acid in aqueous solution: Effects of pH and mixing ratio, *Colloids Surf., B*, 2021, **203**, 111758.
37 W. Wijaya, A. R. Patel, A. D. Setiowati and P. Van der Meeren, Functional colloids from proteins and polysaccharides for food applications, *Trends Food Sci. Technol.*, 2017, **68**, 56–69.
38 Q. Wang, T. Chen, S. Yan, Y. Li and B. Qi, Segregative phase separation of protein/polysaccharide mixed systems: Phase separation mechanisms, characterization technologies, influencing factors, and food applications—a review, *Food Res. Int.*, 2025, **208**, 116240.
39 E. Ghorbani Gorji, A. Waheed, R. Ludwig, J. L. Toca-Herrera, G. Schleining and S. Ghorbani Gorji, Complex coacervation of milk proteins with sodium alginate, *J. Agric. Food Chem.*, 2018, **66**, 3210–3220.
40 J.-R. Han, J.-N. Yan, Y.-N. Du, H.-T. Wu and B.-W. Zhu, Formation and stability of electrostatic complexes formed between scallop female gonad protein isolates and sodium alginate: Influence of pH, total concentration, blend ratio, and ionic strength, *J. Food Sci.*, 2022, **87**, 2504–2514.
41 J. Feng, H. Tian, X. Chen, X. Cai, X. Shi and S. Wang, Interaction between fish gelatin and tremella polysaccharides from aqueous solutions to complex coacervates: Structure and rheological properties, *Food Hydrocolloids*, 2023, **138**, 108439.
42 J.-C. Liu, B. Nie, Y.-Q. Wang, J.-N. Yan and H.-T. Wu, Phase behavior and synergistic gelation of scallop (*Patinopecten yessoensis*) male gonad hydrolysates and gellan gum driven by pH, *J. Sci. Food Agric.*, 2025, **105**, 1841–1849.
43 S. Naji-Tabasi and S. M. A. Razavi, New studies on basil (*Ocimum bacilicum* L.) seed gum: Part III – Steady and dynamic shear rheology, *Food Hydrocolloids*, 2017, **67**, 243–250.
44 Y.-N. Du, J.-N. Yan, S.-Q. Xu, H.-X. Liu, Y.-Q. Wang, B. Lai, C. Wang and H.-T. Wu, Gelation properties and molecular dynamics simulation of thermally induced large yellow croaker (*Pseudosciaena crocea*) roe protein isolate gels, *LWT*, 2023, **189**, 115393.
45 X. Yang, A. Li, D. Li, Y. Guo and L. Sun, Applications of mixed polysaccharide-protein systems in fabricating multi-structures of binary food gels—A review, *Trends Food Sci. Technol.*, 2021, **109**, 197–210.
46 C. J. F. Souza, C. S. F. Souza, L. P. Heckert Bastos and E. E. Garcia-Rojas, Interpolymer complexation of egg white proteins and carrageenan: Phase behavior, thermodynamics and rheological properties, *Int. J. Biol. Macromol.*, 2018, **109**, 467–475.
47 G.-Y. Li, Q.-H. Chen, C.-R. Su, H. Wang, S. He, J. Liu, A. Nag and Y. Yuan, Soy protein-polysaccharide complex coacervate under physical treatment: Effects of pH, ionic strength and polysaccharide type, *Innovative Food Sci. Emerging Technol.*, 2021, **68**, 102612.
48 Y.-Q. Wang, J.-N. Yan, Y.-N. Du, S.-Q. Xu, Z.-J. Zhang, B. Lai, C. Wang and H.-T. Wu, Formation and microstructural characterization of scallop (*Patinopecten yessoensis*) male gonad hydrolysates/sodium alginate coacervations as a function of pH, *Int. J. Biol. Macromol.*, 2023, **253**, 126508.
49 Z. Wang, Y. Du, S. Zhang, J. Hu, Z. Wang, Z. Guo and H. Yang, Mechanism of xanthan gum in inhibiting aggregation in soy protein isolate gels after commercial Sterilization: Implications for texture-modified food for dysphagia, *Food Hydrocolloids*, 2025, **168**, 111481.
50 T.-T. Chen, D. Liu, L.-Q. Li, M.-Y. Jin, Y.-H. Yu and J.-K. Yan, Enhancement of gel characteristics of curdlan thermo-irreversible gels by β-cyclodextrin and its possible mechanisms, *Food Chem.*, 2025, **467**, 142320.
51 Y. Zhang, X. Li, Y. Ge, Y. Hu, R. Zhu, X. Yang, S. Chen, H. Peng and C. Wang, Blueberry leaf polysaccharide/gelatin composite gel: Preparation, characterization, and formation mechanism, *Int. J. Biol. Macromol.*, 2025, **304**, 141020.
52 Q. Li, H. Jin, X. Zhang, G. Hu, C. Lei, H. Sun, L. Sheng, Y. Jin, X. Huang, L. Lu and Z. Cai, Effect of salt penetration and water migration on cooked salted egg yolk gel during storage: Physicochemical properties, structural characteristics and flavor changes, *Food Chem.*, 2023, **404**, 134510.
53 Z. Guo, C. Chen, G. Ma, Q. Yu and L. Zhang, LF-NMR determination of water distribution and its relationship with protein-related properties of yak and cattle during postmortem aging, *Food Chem.: X*, 2023, **20**, 100891.
54 S.-Q. Xu, Y.-N. Du, Z.-J. Zhang, J.-N. Yan, J.-J. Sun, L.-C. Zhang, C. Wang, B. Lai and H.-T. Wu, Gel properties and interactions of hydrogels constructed with low acyl gellan gum and puerarin, *Carbohydr. Polym.*, 2024, **326**, 121594.
55 C. Guo, M. Zhang and H. Chen, Suitability of low-field nuclear magnetic resonance (LF-NMR) combining with back propagation artificial neural network (BP-ANN) to predict printability of polysaccharide hydrogels 3D printing, *Int. J. Food Sci. Technol.*, 2021, **56**, 2264–2272.
56 Z. Ge, D. Yin, Z. Li, X. Chen and M. Dong, Effects of commercial polysaccharides stabilizers with different charges on textural, rheological, and microstructural characteristics of set yoghurts, *Foods*, 2022, **11**, 1764.
57 J. Rahbani, A. R. Behzad, N. M. Khashab and M. Al-Ghoul, Characterization of internal structure of hydrated agar and gelatin matrices by cryo-SEM, *Electrophoresis*, 2013, **34**, 405–408.
58 B. Nie, Y.-N. Du, S.-Q. Xu and H.-T. Wu, Improvement of low-acyl gellan gum on gelation and microstructural properties of protein hydrolysates from male gonad of scallop (*Patinopecten yessoensis*), *Food Chem.*, 2022, **371**, 131114.
59 C. Yang, X. Wang, H. Hu, Y. Feng, H. Tang, W. Zhang and J. Wang, Cold-set oat protein isolate–gellan gum binary gels with various microstructures: Fabrication,

characterization, formation mechanism, and controlled release properties, *Food Hydrocolloids*, 2022, **131**, 107818.

60 J. Babaei, F. Khodaiyan and M. Mohammadian, Effects of enriching with gellan gum on the structural, functional, and degradation properties of egg white heat-induced hydrogels, *Int. J. Biol. Macromol.*, 2019, **128**, 94–100.

61 J. A. Pires Vilela, Â. L. F. Cavallieri and R. Lopes da Cunha, The influence of gelation rate on the physical properties/structure of salt-induced gels of soy protein isolate–gellan gum, *Food Hydrocolloids*, 2011, **25**, 1710–1718.

62 M. Y. Erturk, J. C. Bonilla and J. Kokini, Relationship of non-linear rheological properties and quantitative network analysis parameters as a function of increasingly large amplitude deformations in non-fat, low-fat and high-fat yogurt products, *Food Hydrocolloids*, 2021, **111**, 106194.

63 X. Xu, Q. Han, J. Shi, H. Zhang and Y. Wang, Structural, thermal and rheological characterization of bovine serum albumin binding with sodium alginate, *J. Mol. Liq.*, 2020, **299**, 112123.

64 X. Liu, X. Qin, Y. Wang and J. Zhong, Physicochemical properties and formation mechanism of whey protein isolate-sodium alginate complexes: Experimental and computational study, *Food Hydrocolloids*, 2022, **131**, 107786.